

## GaN Nanowire Functionalized with Atomic Layer Deposition Techniques for Enhanced Immobilization of Biomolecules

D. J. Guo,<sup>†</sup> A. I. Abdulagatov,<sup>‡</sup> D. M. Rourke,<sup>§</sup> K. A. Bertness,<sup>§</sup> S. M. George,<sup>‡</sup> Y. C. Lee,<sup>†,||</sup>  
and W. Tan<sup>\*,†,⊥</sup>

<sup>†</sup>Department of Mechanical Engineering, and <sup>‡</sup>Department of Chemistry and Biochemistry, University of Colorado at Boulder, Boulder, Colorado, <sup>§</sup>National Institute of Standards and Technology Optoelectronics Division, Boulder, Colorado, <sup>||</sup>DARPA Center for Integrated Micro/Nano-Electromechanical Transducers (iMINT), Boulder, Colorado, and <sup>⊥</sup>Departments of Bioengineering and Pediatrics-Cardiology, University of Colorado at Denver, Aurora, Colorado

Received August 20, 2010. Revised Manuscript Received September 27, 2010

We report the use of atomic layer deposition (ALD) coating as a nanobiosensor functionalization strategy for enhanced surface immobilization that may enable higher detection sensitivity. Three kinds of ALD coating films, Al<sub>2</sub>O<sub>3</sub>, TiO<sub>2</sub>, and SiO<sub>2</sub>, were grown on the gallium nitride nanowire (GaN NW) surfaces and characterized with high-resolution transmission electron microscopy (HRTEM) and vacuum Fourier transform infrared spectroscopy (FTIR). Results from HRTEM showed that the thicknesses of ALD-Al<sub>2</sub>O<sub>3</sub>, ALD-TiO<sub>2</sub> and ALD-SiO<sub>2</sub> coatings were 4–5 nm, 5–6 nm, and 12–14 nm, respectively. Results from FTIR showed that the OH contents of these coatings were, respectively, ~6.9, ~7.4, and ~9.3 times that of piranha-treated GaN NW. Furthermore, to compare protein attachments on the different surfaces, poly(ethylene glycol) (PEG)-biotin was grafted on the OH-functionalized GaN NW surfaces through active Si–Cl functional groups. Streptavidin protein molecules were then attached to the biotin ends via specific binding. The immobilized streptavidin molecules were examined with scanning electron microscopy, HRTEM, and fluorescent imaging. Results from HRTEM and energy-dispersive X-ray revealed that the nitrogen concentrations on the three ALD coatings were significantly higher than that on the piranha-treated surface. Results from fluorescent imaging further showed that the protein attachments on the Al<sub>2</sub>O<sub>3</sub>, TiO<sub>2</sub>, and SiO<sub>2</sub> ALD coatings were, respectively, 6.4, 7.8, and 9.8 times that of piranha-treated surface. This study demonstrates that ALD coating can be used as a functionalization strategy for nanobiosensors because it is capable of creating functional groups with much higher density compared to widely used acid modifications, and among the three ALD coatings, ALD-SiO<sub>2</sub> yielded the most promising results in OH content and protein attachment.

### 1. Introduction

Nanomaterial-based biosensors are an exciting research area since nanomaterials are promising for enhancing biosensing capability. Previous studies explored the possibility of using nanostructures such as carbon nanotubes (CNTs),<sup>1</sup> Si nanowires (NWs),<sup>2</sup> and ZnO NWs<sup>3</sup> as sensitive transducers for the detection of biomolecules, including simple structured DNA molecules and sophisticatedly structured proteins.<sup>4,5</sup> Results from these studies demonstrated that 1-dimensional NWs provide sensitivity in transducing binding of low-concentrated biomolecules into electrical signals. The sensitivity of these nanomaterials was attributed to their high surface-to-volume ratio and their capability of altering electrical conductivity upon small molecule binding. Gallium nitride (GaN) NWs have emerged as an attractive semiconductor material. GaN NWs possess outstanding thermal and chemical stability and optoelectronic properties, which enable application for the detection of biomolecules.<sup>6</sup> Furthermore, GaN NWs were used as electrical nanogenerators via intrinsic piezoelectric

properties.<sup>7</sup> The piezoelectric property might also be desired for biosensing as a small deformation of the NW can be transformed into electrical signals.<sup>7</sup> Additionally, GaN NWs are also of potential use as a high electron mobility material to detect the interaction between biomolecules of proteins and DNA,<sup>8</sup> since almost all biomolecules are positively or negatively charged.<sup>4</sup> Because GaN NWs offer these advantages over other transducer materials and the physiological environments where biosensors are applied for in situ protein detections are often sophisticated, GaN NWs are good candidates for biosensing transducers.<sup>9</sup>

In addition to the selection of the transducer substrate, functionalization of nanomaterials to facilitate surface attachment of recognition molecules is also critical not only for sensing performance, but also for detection reliability. Previous studies employed covalent or noncovalent functionalization techniques to mediate grafting of proteins onto CNT or NW surfaces.<sup>1</sup> Different from these substrates, the surface of GaN NWs readily presents some active groups such as Ga–O–H group or Ga–H group for grafting.<sup>9–12</sup> To produce denser OH groups for surface

\*Correspondence should be sent to Wei Tan, wtan@Colorado.Edu.

(1) Gruner, G. *Anal. Bioanal. Chem.* **2006**, *384*, 322.

(2) Cui, Y.; Wei, Q.; Park, H.; Lieber, C. M. *Science* **2001**, *293*, 1289.

(3) Yeh, P. H.; Li, Z.; Wang, Z. L. *Adv. Mater.* **2009**, *21*, 4975.

(4) Chen, R. J.; Bangsaruntip, S.; Drouvalakis, K. A.; Kam, N. W. S.; Shim, M.; Li, Y. M.; Kim, W.; Utz, P. J.; Dai, H. J. *Proc. Natl. Acad. Sci. U.S.A.* **2003**, *100*, 4984.

(5) Star, A.; Gabriel, J. C.; Bradley, K.; Gruner, G. *Nano Lett.* **2003**, *3*, 459.

(6) Chen, C. P.; Ganguly, A.; Wang, C. H.; Hsu, C. W.; Chattopadhyay, S.; Hsu, Y. K.; Chang, Y. C.; Chen, K. H.; Chen, L. C. *Anal. Chem.* **2009**, *81*, 36.

(7) Huang, C. T.; Song, J. H.; Lee, W.; Fan, D.; Ding, Y.; Gao, Z.; Hao, Y.; Chen, L. J.; Wang, Z. L. *J. Am. Chem. Soc.* **2010**, *132*(13), 4766.

(8) Alur, S.; Gnanaprakasa, T.; Xu, H.; Wang, Y.; Simonian, A. L.; Oyarzabal, O. A.; Park, M. CS MANTECH Conference, **2009**, Florida, USA.

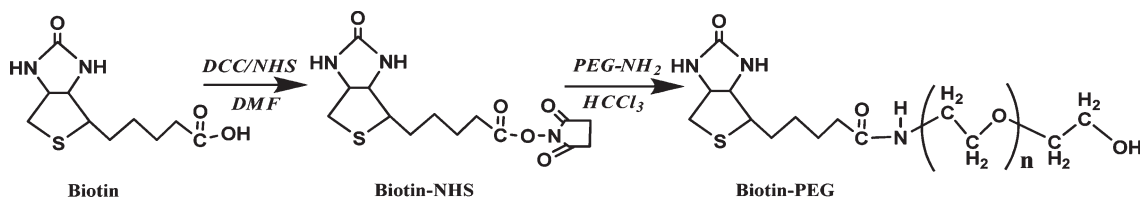
(9) Ganguly, A.; Chen, C. P.; Lai, Y. T.; Kuo, C. C.; Hsu, C. W.; Chen, K. H.; Chen, L. C. *J. Mater. Chem.* **2009**, *19*, 928.

(10) Brandt, M. S.; Ager, J. W., III; Gtz, W.; Johnson, N. M.; Harris, J. S.; Molnar, R. J., Jr.; Moustakas, T. D. *Phys. Rev. B* **1994**, *49*, 14758.

(11) Baur, B.; Steinhoff, G.; Hernandez, J.; Purruicker, O.; Tanaka, M.; Nickel, B.; Stutzmann, M.; Eickhoff, M. *Appl. Phys. Lett.* **2005**, *87*, 263901.

(12) Seager, C. H.; Myers, S. M.; Petersen, G. A.; Han, J.; Headley, T. J. *Appl. Phys.* **1999**, *85*, 2568.

Scheme 1. Reaction Routes of Biotin-NHS and PEG-Biotin



functionalizations, GaN NWs are usually treated by oxidizing acids such as the mixture of  $\text{H}_2\text{SO}_4/\text{H}_2\text{O}_2$  (piranha etch) or the mixture of  $\text{H}_2\text{SO}_4/\text{HNO}_3$ . In addition to grafting biomolecules directly with active OH, a silanization technique is also used to graft biomolecules through an intermediate organic monolayer. Chen et al. demonstrated the silanization approach to immobilize DNA on a GaN NW for the detection of DNA hybridization.<sup>6,9</sup> Eickhoff et al. also used a similar approach to immobilize enzymes onto a stripped GaN belt for a field-effect transistor, which resulted in an intense detection signal-to-noise ratio.<sup>13,14</sup> However, the common technique using oxidative acids with or without an organic monolayer changes the intrinsic property of the NW or CNT. Also, acid treatments are often accompanied by heat or sonication, which may result in unexpected breaking of the NWs from their matrix substrates. Furthermore, the resultant OH groups on the surface have seldom been directly characterized or quantified. Instead, the demonstration of OH function was done indirectly by characterizing the organic monolayer with X-ray photoelectron spectroscopy.<sup>15</sup> Because the number of grafted biomolecules is proportional to the number of surface active groups on the GaN NW surface, it is essential to have a mechanistic approach to quantify and increase the density of surface active groups for enhanced sensing and transducing performances.

Atomic layer deposition (ALD) is useful for coating nanomaterials.<sup>16,17</sup> ALD utilizes sequential, self-limiting surface chemical reactions to achieve atomic layer controlled thin film growth.<sup>18</sup> After completing ALD oxide deposition where water is used as an oxygen source, the surface is left with a high concentration of  $-\text{OH}$  species,<sup>19</sup> thus providing a potential strategy to graft highly dense biomolecules. Films grown with ALD are typically dense, pinhole-free, uniform, and extremely conforming to the underlying substrate. Additionally, the coating process is relatively benign to GaN NWs. Therefore, this study exploits this technique as a coating strategy for biosensing. The ALD technology was compared with the acid treatment technique in terms of the biomolecule attachment on GaN NW surface. To evaluate the performances, a widely used specific biomolecule recognition biotin–streptavidin model was employed,<sup>20</sup> and Fourier transform infrared spectroscopy (FTIR), high-resolution transmission electron microscopy (HRTEM), scanning electron microscopy (SEM), fluorescence imaging, and atomic force microscopy

(Supporting Information) were used to characterize the functionalized surfaces.

## 2. Experimental Section

### 2.1. Materials and Material Preparations.

O-(2-Aminoethyl) poly(ethylene glycol) 3000 (PEG-NH<sub>2</sub>), dicyclohexylcarbodiimide (DCC), *N*-hydroxysuccinimide (NHS), silicon tetrachloride (SiCl<sub>4</sub>), triethylamine, uranyl acetate (UA), trimethylaluminum (TMA, Al<sub>2</sub>(CH<sub>3</sub>)<sub>6</sub>), pure silanol, dry *N,N*-dimethylformamide (DMF), diether, CH<sub>2</sub>Cl<sub>2</sub>, and chloroform were obtained from Sigma-Aldrich Inc. (St Louis, MO). TMA (99.8%) was obtained from Strem Chemical, Inc. (Newburyport, MA). Biotin, streptavidin, and Cy-3 labeled streptavidin were obtained from Fisher Scientific Inc. (Pittsburgh, PA).

Preparation of biotin NHS-ester (NHS-biotin) was performed as follows. First, 0.26 g of NHS (2.5 mMol) and 0.51 g of DCC (2.5 mMol) were put into 50 mL pure DMF of biotin (0.5 g, 2.05 mMol), and reacted by stirring at 50 °C for 16 h. After the reaction, the undissolved substance was filtered off. Drops of diether were then added to the filtrate solution to produce a white precipitate of NHS-biotin. The yield of this process was ~95%, determined based on the FTIR spectra at 3228, 3108, 3063, 2939, 2915, 2875, 2846, 1818, 1787, 1745, 1729, and 1696 cm<sup>-1</sup> (Supporting Information s-Figure 1). This reaction is illustrated in Scheme 1.

Preparation of PEG functionalized biotin (PEG-biotin) was performed as follows.<sup>21</sup> First, 0.225 g of NHS-biotin (0.67 mMol) was added into 50 mL pure chloroform solution of PEG-NH<sub>2</sub> (1.0 g, 0.33 mMol). Then, excessive triethylamine was added into this solution to accelerate the reaction. The reaction was performed in the dark at room temperature for 6 h. After the reaction, the excessive NHS-biotin and some undissolved substances were filtered off. Drops of diether were then added to the filtrate solution to produce white precipitate. Finally, the precipitate was recrystallized with dry diether. The yield of PEG-biotin from biotin was ~90%, determined based on the FTIR spectra at 3340, 2978, 2945, 2883, 2857, 2806, 2739, 1702, 1698, and 1667 cm<sup>-1</sup> (Supporting Information s-Figure 1). This reaction was illustrated in Scheme 1.

### 2.2. Surface Functionalization.

Two approaches to NW surface functionalizations were designed (Scheme 2). One approach is to use piranha solution to treat GaN NWs for OH functionalization on the surface. The other approach uses an ALD technique to produce active OH groups on the GaN surface. Three kinds of ALD coating films (Al<sub>2</sub>O<sub>3</sub>, SiO<sub>2</sub>, and TiO<sub>2</sub>) were employed. After OH functionalization, three steps were involved in attaching streptavidin proteins to the GaN NWs: (a) the formation of Si–Cl functionalized NWs; (b) the formation of biotin functionalized NWs; and (c) the attachment of streptavidin on NWs through biotin/streptavidin recognition. Herein, the NW samples immediately after the treatments with piranha solution, ALD-Al<sub>2</sub>O<sub>3</sub>, ALD-TiO<sub>2</sub> and ALD-SiO<sub>2</sub> coatings were labeled as samples a, b, c, and d, respectively; their biotin-functionalized NW samples were labeled as samples e, f, g, and h, respectively; and their streptavidin-grafted samples were labeled as samples i, j, k, and l, respectively.

Preparation of Si–Cl functionalized GaN NWs was performed according to the method described previously.<sup>22</sup> The OH-functionalized as-grown GaN chip of 1 cm in diameter was

(13) Steinhoff, G.; Purrucker, O.; Tanaka, M.; Stutzmann, M.; Eickhoff, M. *Adv. Funct. Mater.* **2003**, *13*, 841.

(14) Baur, B.; Steinhoff, G.; Hernandez, H.; Purrucker, O.; Tanaka, M.; Nickel, B.; Stutzmann, M.; Eickhoff, M. *Appl. Phys. Lett.* **2005**, *87*, 263901.

(15) Baur, B.; Howgate, J.; von Ribbeck, H.-G.; Gawlina, Y.; Bandalo, V.; Steinhoff, G.; Stutzmann, M.; Eickhoff, M. *Appl. Phys. Lett.* **2006**, *89*, 183901.

(16) Cavanagh, A. S.; Wilson, C. A.; Weimer, A. W.; George, S. M. *Nanotechnology* **2009**, *20*, 255602.

(17) Herrmann, C. F.; Fabreguette, F. H.; Finch, D. S.; Geiss, R.; George, S. M. *Appl. Phys. Lett.* **2005**, *87*, 123110.

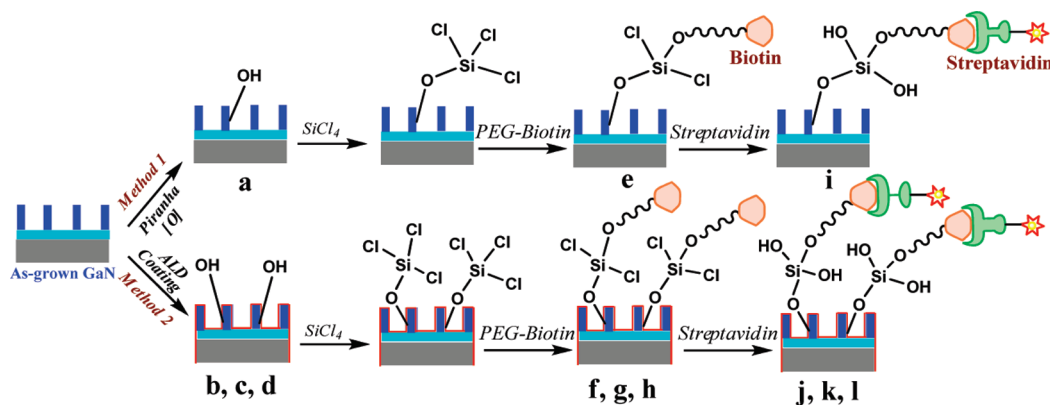
(18) George, S. M. *Chem. Rev.* **2010**, *110*, 111.

(19) Dillon, A. C.; Dillon, A. C.; Ott, A. W.; Way, J. D.; George, S. M. *Surf. Sci.* **1995**, *322*, 230.

(20) González, M.; Bagatolli, L. A.; Echabe, I.; Arrondo, J. L. R.; Argaran, C. E.; Cantor, C. R.; Fidelio, G. D. *J. Biol. Chem.* **1997**, *272*, 11288.

(21) Anne, A. *Tetrahedron Lett.* **1998**, *39*, 561.

(22) Popat, K. C.; Mor, G.; Grimes, C. A.; Desai, T. A. *Langmuir* **2004**, *20*, 8035.

Scheme 2. Two Approaches for Immobilizing Streptavidin<sup>a</sup>

<sup>a</sup> (1) An as-grown GaN chip with upright GaN NWs on the surface was oxidized with a piranha solution. (2) Using ALD techniques, three kinds of ALD coatings, i.e., SiO<sub>2</sub>, Al<sub>2</sub>O<sub>3</sub>, and TiO<sub>2</sub>, were formed on GaN NW surfaces. Subsequent modification steps were similar: The chip was incubated in a pure SiCl<sub>4</sub> solution forming a Si–Cl linker which reacted with PEG-biotin. Finally, Cy-3 labeled streptavidin proteins attached to the surface. Herein, the NW samples immediately after the treatments with piranha solution, ALD-Al<sub>2</sub>O<sub>3</sub>, ALD-TiO<sub>2</sub> and ALD-SiO<sub>2</sub> coatings were labeled as samples a, b, c, and d, respectively; their biotin functionalized NW samples were labeled as samples e, f, g, and h, respectively; and their streptavidin-grafted samples were labeled as samples i, j, k, and l, respectively.

placed in a sealed container with ~2 mL pure SiCl<sub>4</sub> solution and incubated for 1 h at room temperature. The GaN NW chip was then taken out quickly, washed with excessive dry chloroform for three times, and dried with dry air.

Preparation of biotin-functionalized GaN NWs was performed as follows. The newly formed Si–Cl functionalized GaN NW chip was immersed in the dry chloroform solution containing PEG-biotin (0.3 g in 2 mL). A small quantity of triethylamine was then added into the solution. The reaction lasted for ~1 h in the dark. The GaN NW chip was then retrieved, washed with dry chloroform three times, and dried with air.

Streptavidin attachment was performed according to the method described previously.<sup>23</sup> The biotin-functionalized GaN NW chip was immersed in the streptavidin solution (0.1 mg/1 mL in deionized water) or the Cy-3 labeled streptavidin solution (1/100 v/v of streptavidin in deionized water) for 30 min. The chip was then taken out, washed with deionized water three times, and dried with air.

**2.3. Growth of GaN NWs.** As-grown GaN NW chips were fabricated using the molecular beam epitaxy technique under the condition of a high substrate temperature (~800 °C) and a high N<sub>2</sub> plasma flux at radio frequency. All N species come from the plasma N<sub>2</sub> source. Additional details of the growth conditions were reported elsewhere.<sup>24,25</sup>

**2.4. ALD Coating on GaN NWs.** All ALD films were deposited at 120 °C in a hot walled viscous-flow reactor described in detail elsewhere.<sup>26</sup> ALD of Al<sub>2</sub>O<sub>3</sub> and TiO<sub>2</sub> were achieved using trimethylaluminum (Al<sub>2</sub>(CH<sub>3</sub>)<sub>6</sub>), titanium tetrachloride (TiCl<sub>4</sub>), and water.<sup>27,28</sup> Chromatography-grade water was used after several cycles of freeze–pump–thaw. The ALD-SiO<sub>2</sub> was deposited in so-called “rapid” mode using tris(*tert*-pentoxy)silanol.<sup>29</sup> Prior to TiO<sub>2</sub> and SiO<sub>2</sub> deposition, ALD-Al<sub>2</sub>O<sub>3</sub> was predeposited on gallium nanowires as a seed layer in order to facilitate TiO<sub>2</sub> and SiO<sub>2</sub> nucleation. For ALD-Al<sub>2</sub>O<sub>3</sub> coating, the number of

deposition cycles was 65 and the typical growth rate was around ~0.1 nm/cycle. For ALD-TiO<sub>2</sub> coating, after 20 cycles of Al<sub>2</sub>O<sub>3</sub> coating, TiO<sub>2</sub> was coated for 80 cycles with a typical growth rate of ~0.06 nm/cycle. For ALD-SiO<sub>2</sub> coating, after 50 cycles of Al<sub>2</sub>O<sub>3</sub> coating, SiO<sub>2</sub> was coated for 1 cycle with a growth rate of ~12 nm/cycle. Therefore, the estimated film thicknesses are ~7–8 nm for ALD-Al<sub>2</sub>O<sub>3</sub>, ~6–8 nm for ALD-TiO<sub>2</sub>, and ~15–18 nm for ALD-SiO<sub>2</sub>.

**2.5. Characterization with FTIR-IR.** Infrared spectra were recorded on a vacuum Bruker Vertex 80 instrument (Bruker Corporation, Germany) at 1 cm<sup>-1</sup> resolution with a deuterated triglycine sulfate detector. Typically, 128 scans were acquired per spectrum under a vacuum pressure of ~130 Pa. A blank crystal KBr disk with a small, round pit at the center was used to place GaN NWs and to obtain the background spectrum. All GaN NW samples were removed from their as-grown chips by sonication and dispersed into CH<sub>2</sub>Cl<sub>2</sub> solution. Drops of this dispersed NW solution were then pipetted onto the KBr disk and dried in an oven at 80 °C for 1 h to remove the CH<sub>2</sub>Cl<sub>2</sub> solution. The disk samples carried by KBr were mounted in a purged sample chamber. To evaluate the surface density of molecular monolayers, IR spectra in both transmittance mode and absorbance mode were obtained.

**2.6. Electron Microscopy Imaging.** Field emission scanning electron microscopy (FE-SEM) and HRTEM were both used. FE-SEM imaging was performed on a LEO 1530VP instrument (LEO Corporation, Germany) for the topographical structure of as-grown GaN NW. An accelerating voltage of 5.0 kV was used with a Schottky field emission source. Both planar and cross-sectional views of GaN NWs were obtained. HRTEM was performed on a JEM2000EX instrument (JEOL Ltd., Japan) using an accelerating voltage of 200 kV. A copper microgrid was used to carry the dispersed NWs for HRTEM observations. For ungrafted GaN NWs, GaN NWs were removed from the chips and dispersed into a CH<sub>2</sub>Cl<sub>2</sub> solution. Then, 10 μL of the dispersed solution was dropped onto a Cu microgrid and dried in vacuum. For streptavidin-grafted GaN NWs, the microgrid was dyed with 1% UA solution after drying. This is performed by adding three drops of 10 μL UA solution on a clean substrate, and then placing the Cu microgrid on top of it for ~10 s. After that, the Cu microgrid was taken out, washed with 100 μL deionized water, and dried. Samples a–d and i–l were characterized with HRTEM and energy-dispersive X-ray (EDX) analyses. EDX data were collected by a Si(Li) detector and were analyzed with the built-in software. In each EDX analysis, the surface information such as the atom quantity and the mass of N,

(23) Holmberg, A.; Blomstergren, A.; Nord, O.; Lukacs, M.; Lundeberg, J.; Uhlén, M. *Electrophoresis* **2005**, *26*, 501.

(24) Bertness, K. A.; Roshko, A.; Mansfield, L. M.; Harvey, T. E.; Sanford, N. A. *J. Cryst. Growth* **2008**, *310*, 3154.

(25) Tanner, S. M.; Gray, J. M.; Rogers, C. T.; Bertness, K. A.; Sanford, N. A. *Appl. Phys. Lett.* **2007**, *91*, 203117.

(26) Elam, J. W.; Groner, M. D.; George, S. M. *Rev. Sci. Instrum.* **2002**, *73*, 2981.

(27) Groner, M. D.; Fabreguette, F. H.; Elam, J. W.; George, S. M. *Chem. Mater.* **2004**, *16*, 639.

(28) Ritala, M.; Leskelä, M.; Nykänen, E.; Soininen, P.; Niinistö, L. *Thin Solid Films* **1993**, *225*, 288.

(29) Burton, B. B.; Boleslawski, M. P.; Desombre, A. T.; George, S. M. *Chem. Mater.* **2008**, *20*, 7031.

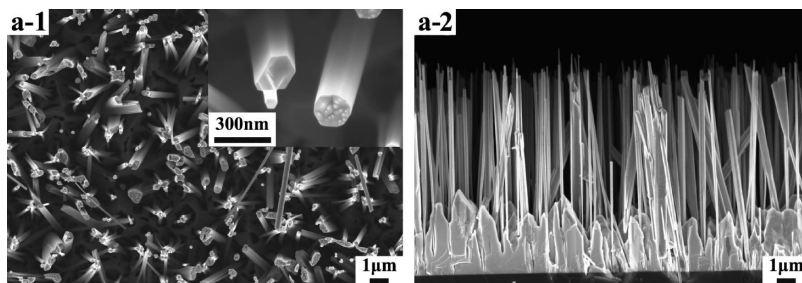


**Figure 1.** SEM images show the top-view (a-1) and cross-sectional view (a-2) of the as-grown GaN NW chip.

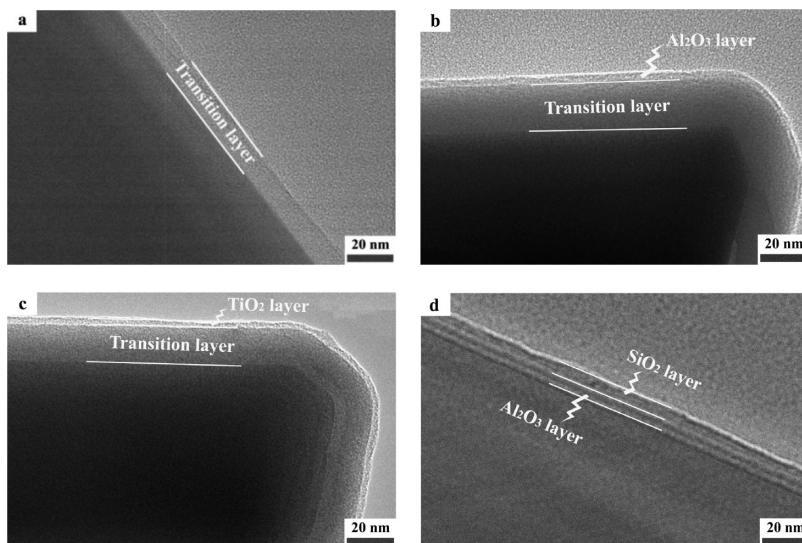


**Figure 2.** HRTEM images of samples a, b, c, and d.

Ga, Si, Al, and Ti at  $\sim 300$  nm was collected to demonstrate the reaction of PEG-biotin and the subsequent attachment of streptavidin.

### 2.7. Fluorescent Imaging of Cy-3 Labeled Streptavidin.

Biotin-functionalized GaN NWs were incubated with Cy-3 labeled streptavidin; the samples were washed with deionized water three times and then placed under a fluorescence microscope (Carl Zeiss Inc., Germany). Images with a  $450 \times 400 \mu\text{m}^2$  area were collected. To avoid the spatial variation, all samples were dispersed onto the crystal Si surface with a similar thickness. The upright GaN NWs and the GaN NWs, after treatments with piranha or three kinds of ALD coating, were all analyzed to determine the attachment of streptavidin. The fluorescent intensity of streptavidin molecules is quantified with *Photoshop 7.0*. For data collection, 10–13 points were selected from 4 images of each sample. Data collected were statistically analyzed using the one-way ANOVA test. Student's *t* test was then used to compare the means of each individual group. The level of significance was set at  $\alpha = 0.05$  for 95% statistical significance. Error bars on all the histogram charts represent the standard error of the mean based on the total number of the samples.

## 3. Results and Discussion

### 3.1. Characterizations of As-Grown GaN with FESEM.

FESEM was used to characterize the morphology of as-grown GaN NWs (sample a). Typical FESEM images of as-grown GaN NWs treated with the piranha solution are shown in Figure 1. The top-view image shows that the upright GaN NWs are uniformly grown on a Si substrate. The image with a high magnification demonstrates that each GaN NW exhibits a single column-shaped morphology, and each prismatic plane exhibits a fairly smooth

surface. The cross-sectional view demonstrates a densely packed array of GaN NWs on the chip. It can be estimated from the images that GaN NWs exhibit length of 9–10  $\mu\text{m}$ , and their pitches are less than 1  $\mu\text{m}$ . The GaN NWs can be removed from the matrix chip through sonication in dimethylformamide or  $\text{CH}_2\text{Cl}_2$  solution. Removed GaN NWs were used for FTIR, HRTEM, and fluorescence characterizations.

### 3.2. Characterizations of ALD Coating with HRTEM.

To characterize different ALD coatings, GaN NWs (samples a–d) were observed with HRTEM (Figure 2). Figure 2a shows the TEM image of piranha-treated GaN NWs. The dark side shows the bulk GaN as a relatively dense layer, and the light side shows the Cu microgrid, which is composed of numerous fine particles. Between them, there is a transition layer with a thickness of  $\sim 12$  nm. As shown in Figure 1, the vertical GaN NW exhibits a smooth morphology and generally grows with hexagonal cross section. This transition layer may come from the prismatic plane of GaN NW. Figure 2b shows the image of  $\text{Al}_2\text{O}_3$ -coated GaN NWs. A uniform ALD layer of  $\text{Al}_2\text{O}_3$  film with a thickness of 5–6 nm is identified. According to EDX results, the atomic ratio of Al is 34%. Between the ALD layer and the dark GaN bulk, there is a transition layer with a thickness of  $\sim 23$  nm. Figure 2c shows the image of  $\text{TiO}_2$ -coated GaN NWs. A uniform ALD coating layer of  $\text{TiO}_2$  film with a thickness of 4–5 nm is identified. This layer has a high Ti concentration, as EDX results show the atomic ratio of Ti is 30%. Similar to  $\text{Al}_2\text{O}_3$ -coated GaN NWs, there is a transition layer with a thickness of  $\sim 20$  nm. As described in the Experimental Section,  $\text{TiO}_2$  film was grown on adhesion layer of  $\text{Al}_2\text{O}_3$  film. EDX results show the atomic ratio of Al is 9%.

Therefore, a double layer showing  $\text{TiO}_2$  and  $\text{Al}_2\text{O}_3$  film is expected. However, the two layers cannot be distinguished here, probably because they are extremely thin and the  $\text{Al}_2\text{O}_3$  film is concealed by the GaN NW surface and  $\text{TiO}_2$  coating layer. Figure 2d shows the image of  $\text{SiO}_2$ -coated GaN NWs. According to EDX results, the atomic ratio of Si is 26% and that of Al is 24%. Different from  $\text{TiO}_2$ -coated GaN NWs shown in Figure 2b, a two-layer structure are clearly shown here. The bottom layer shows  $\text{Al}_2\text{O}_3$  coating with a thickness of 5–6 nm, while the top layer shows  $\text{SiO}_2$  coating with a thickness of 7–8 nm. No clear transition layer is evident, since it may be difficult for the electron beam to penetrate through the two dense layers when the GaN NW surface is upright to the Cu grid. Compared to the estimated thicknesses ( $\sim 7$ –8 nm for ALD- $\text{Al}_2\text{O}_3$ ;  $\sim 6$ –8 nm for ALD- $\text{TiO}_2$ ;  $\sim 15$ –18 nm for ALD- $\text{SiO}_2$ ), the film thicknesses obtained from TEM images were found to be  $\sim 35\%$  less. This can be attributed to precursor diffusion limitations for a high aspect ratio structure such as GaN nanowire. The ALD deposition process optimization is performed by providing sufficient reactants, exposure, and purge times in order to compensate for long diffusion times.

**3.3. Characterizations of Surface Active Functions with Vacuum FTIR.** Although active OH groups were thought to be present on the GaN NW surface,<sup>6,9,13–15</sup> previous studies have not directly characterized them. Compared to other possible detection methods such as XPS, mass spectroscopy, and elemental analysis, FTIR is an effective strategy to characterize OH functionality because the O–H stretching vibration of  $\sim 3200\text{ cm}^{-1}$  and the bending vibration of  $\sim 1600\text{ cm}^{-1}$  are very sensitive and these peaks are almost interference-free. More importantly, the absorbance intensity of the O–H bond can be obtained by counting the peak area according to Beer's law.<sup>30</sup> In addition, the vacuum FTIR spectroscopy is used to characterize surface-active functions and the monolayer subsequently grafted on the GaN NW surface due to the following considerations: (1) Because GaN NW is a kind of low-doped semiconductor, the nanoscale GaN NW allows the IR beam to pass for the absorbance detection. (2) Because the wavelength of the IR beam is in the microscale and the thicknesses of three kinds of ALD coatings (i.e., 5–6 nm, 4–5 nm, and 12–14 nm) are in the nanoscale, the IR beam should be easily transmitted through ALD layers. (3) As the three coating layers are very thin, optical interference can be ignored, and thus, its influence on the integrated areas of the peaks is ignored. (4) The transmission FTIR (TR-FTIR) is convenient for collecting the information from both GaN NWs and ALD coating films. We thus used TR-FTIR to detect the OH content and to monitor the grafting efficiency at each step. (5) Because the vibration peaks of  $\text{CO}_2$  and  $\text{H}_2\text{O}$  significantly influence the IR analysis of the organic monolayer, a vacuum IR was adopted to avoid these noises. As the GaN NW growth substrate is highly doped crystal silicon, the IR beam has difficult penetrating it. Therefore, GaN NWs were removed and dispersed on a KBr disk for TR-FTIR analyses.

To compare the influence of different surface treatments on the OH contents, Samples a–d were analyzed with vacuum FTIR. Their absorbance mode IR curves were shown in Figure 3. All sample curves in this figure exhibited four kinds of IR vibrations, namely, O–H, C–H, Ga–N, and metal–O (M–O). The absorbance intensities of these vibrations change with the samples. For curve 3a, two kinds of active functions of O–H are clearly shown.<sup>31</sup> The vibration of  $3358\text{ cm}^{-1}$  is assigned to the stretching

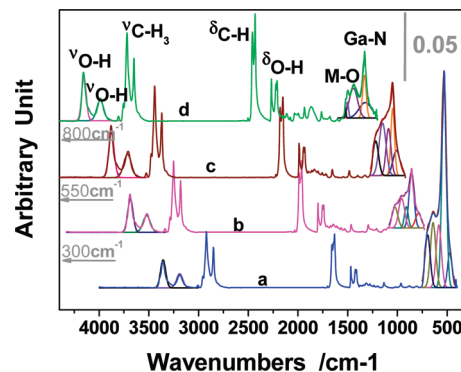


**Figure 3.** Absorbance-mode IR spectra of piranha-treated GaN (a), GaN with ALD- $\text{Al}_2\text{O}_3$  coating (b), GaN with ALD- $\text{TiO}_2$  coating (c), and GaN with ALD- $\text{SiO}_2$  coating (d). Each overlapped peak in the range  $750\text{ cm}^{-1}$ – $400\text{ cm}^{-1}$ , containing Al–O, Ti–O, Si–O, and Ga–N vibration peaks, was fitted with five individual peaks. In particular, a sharp Ga–N stretching peak was analyzed, and its area was calculated using *Origin* software (v 7.5) to compare the OH content among the samples. The spectra were plotted in the wavenumber range  $4000$ – $400\text{ cm}^{-1}$  with marked shifts for clarity.

vibration of O–H derived from H-bonding or physical absorbed water. This O–H vibration is mainly attributed to the water adsorption, because NWs have a high area/volume ratio and thus a high surface energy. The peak at  $3190\text{ cm}^{-1}$  is assigned to the stretching vibration of O–H group derived from the oxidation of piranha solution. As a rigid covalent linker of (Ga)O–H, this O–H group is important to graft an organic monolayer for the attachment of biomolecules. It should be noted that all IR determinations here must be performed in an absolutely dry condition, because trace water molecules could merge these two O–H peaks into one broad peak according to our determinations (Supporting Information s-Figure 2). In the region of  $1690$ – $1490\text{ cm}^{-1}$ , the corresponding O–H bending vibrations with dual peaks are also observed. Similar to the stretching vibrations, trace water molecules could also merge these two O–H peaks into one broad peak (Supporting Information s-Figure 2). Because GaN NWs strongly adsorb hydrocarbon species,<sup>31</sup> C–H stretching vibrations such as peaks at  $2921\text{ cm}^{-1}$  and  $2850\text{ cm}^{-1}$ , and bending vibrations such as those at  $1470\text{ cm}^{-1}$  and  $1411\text{ cm}^{-1}$  appear. Since  $\text{CH}_2\text{Cl}_2$  was used as the dispersant, the C–H peaks show stronger absorbance compared to the curves shown in Supporting Information s-Figure 2. An intense and sharp Ga–N stretching peak is present at  $534\text{ cm}^{-1}$ ,<sup>32</sup> which is shouldered with the Si–O peak derived from the silicon oxide substrate where GaN NW was grown and removed.

In curves 3b, 3c, and 3d, similar peaks are shown. Clearly, the O–H stretching intensity increases compared to that of curve 3a. Metal oxide peaks including Al–O stretching, Ti–O stretching, and Si–O bending in the region  $750$ – $410\text{ cm}^{-1}$  are shown in the corresponding curves and are shouldered with Ga–N stretching band. To compare the OH contents among the samples, the absorbance FTIR was used. As shown above, the OH group at  $\sim 3190\text{ cm}^{-1}$  was adopted to evaluate OH content for functional comparisons. Because the absolute value of the O–H peak area ( $A_{\text{O-H}}$ ) can be affected by many parameters, such as the instrumental setup and the sample amount, another absorbance peak in the same curve is used as an internal reference. Since the sharp Ga–N stretching at  $534\text{ cm}^{-1}$  is the only peak that is not affected by environments, this peak is used as the reference to

(30) Guo, D. J.; Xiao, S. J.; Liu, H. B.; Xia, B.; Chao, J.; Pan, Y.; You, X. Z. *Langmuir* **2005**, *21*, 10487.

(31) Baraton, M. I.; Gonsalves, K. E. J. *Cluster Sci.* **1999**, *10*, 133.

(32) Shoubin Xue, S. B.; Zhang, X.; Huang, R.; Zhuang, H. Z.; Xue, C. S. *J. Chem. Soc., Dalton Trans.* **2008**, 4296.

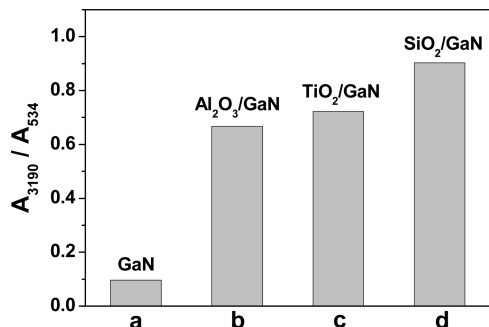


**Figure 4.** Comparison of the densities of OH functional groups on the different samples (samples a–d) using the ratio of the O–H area at 3190  $\text{cm}^{-1}$  to the area of Ga–N at 534  $\text{cm}^{-1}$ . Both areas refer to the peaks shown in the correspondent absorbance FTIR curves.

experimentally compare the OH contents. Besides the Ga–N stretching peak at 534  $\text{cm}^{-1}$ , the overlapping peak in 750–410  $\text{cm}^{-1}$  may contain a Ga–N stretching peak together with other peaks including the stretching peaks of Al–O ( $\sim 725 \text{ cm}^{-1}$  and  $\sim 680 \text{ cm}^{-1}$ ) and Ti–O ( $\sim 600 \text{ cm}^{-1}$ ), and the bending Si–O (485  $\text{cm}^{-1}$ ). The peak is thus fitted with five individual peaks. The Ga–N stretching peak is analyzed. The area of Ga–N stretching peak ( $A_{\text{Ga-N}}$ ) and the ratio of  $A_{\text{O-H}}/A_{\text{Ga-N}}$  for each sample were shown in Supporting Information s-Table 1. For samples a–d, the  $A_{\text{O-H}}/A_{\text{Ga-N}}$  ratios are 0.096, 0.667, 0.722, and 0.903, respectively (Figure 4). Therefore, compared to the OH content on the piranha-treated sample, the functional OH contents on the three ALD coated samples increased  $\sim 6.9$ ,  $\sim 7.4$ , and  $\sim 9.3$  times, respectively. We thus conclude that the OH content after ALD coating is greatly enhanced, and among the three, ALD-SiO<sub>2</sub> shows the best performance.

**3.4. Monitoring Surface Modifications with Vacuum FTIR.** To monitor the PEG–biotin modification step and subsequent recognition of streptavidin, samples e–l were analyzed with vacuum FTIR. Those absorbance-mode IR curves were shown in Supporting Information s-Figure 3. The PEG–biotin functional group on the ALD-SiO<sub>2</sub> GaN NW surface seems to be much denser when compared to the other surfaces. Therefore, the IR spectra on the ALD-SiO<sub>2</sub> GaN NW surfaces were used to illustrate the modification process. Detailed IR spectrum data showing the modification steps on the ALD-SiO<sub>2</sub> GaN NW surface are summarized in Figure 5 and Table 1. Curve 5 h (sample h) shows that PEG–biotin grafted samples exhibit typical PEG-derived C–H<sub>2</sub> stretching peaks at 2887  $\text{cm}^{-1}$  and 2860  $\text{cm}^{-1}$ ,<sup>33</sup> both peaks appear as shoulders on the original C–H<sub>3</sub> peaks derived from adsorbed hydrocarbon compounds. A vibration peak of C=O is present at 1702  $\text{cm}^{-1}$ , and the bending vibration of N–H is present at 1665  $\text{cm}^{-1}$  with a shoulder of O–H bending vibration. These two peaks may be derived from the amide bond from the imidazol ring of biotin. In addition, a new N–H bending peak appears at 1543  $\text{cm}^{-1}$ , and a vibration peak of C=O is present at 1652  $\text{cm}^{-1}$ ; these two peaks may be derived from the amide bond which connects biotin and PEG.<sup>34</sup> Also, two Si–O stretching vibrations appear at 846 and 805  $\text{cm}^{-1}$ , which may be derived from the hydrolysis of Si–Cl.<sup>35</sup> Since the Si–Cl bond is highly active, it easily undergoes hydrolysis when exposed to the air. Also, the Si–Cl bond appears in the range

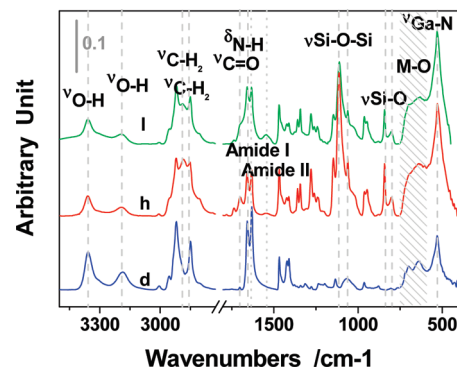


**Figure 5.** Absorbance-mode IR spectra of ALD-SiO<sub>2</sub> GaN NWs (sample d), PEG–biotin functionalized ALD-SiO<sub>2</sub> GaN NWs (sample h), and streptavidin-grafted ALD-SiO<sub>2</sub> GaN NWs (sample l). The wavenumber range is plotted from 3500  $\text{cm}^{-1}$  to 400  $\text{cm}^{-1}$  with a break from 2725  $\text{cm}^{-1}$  to 1805  $\text{cm}^{-1}$ .

500–600  $\text{cm}^{-1}$ , where bands are difficult to assign accurately. Therefore, the IR spectra of Si–Cl functionalized GaN NWs were not discussed. In addition, the vibrations of Si–O–Si at 1072 and 1110  $\text{cm}^{-1}$  increase after PEG–biotin modification. These peaks may be derived from the reaction between Si–Cl and Si–OH. Also, the intensity of O–H bonds is attenuated after PEG–biotin modification. Collectively, all of these results demonstrate that PEG–biotin was successfully grafted on the sample surface. Curve 5 L (sample l) shows the IR spectrum of the samples after the attachment of streptavidin. Typical vibrations of amide I at 1654  $\text{cm}^{-1}$  and amide II at 1546  $\text{cm}^{-1}$  are present,<sup>36</sup> which greatly enhance the intensity of original amide peaks. These results demonstrate the immobilization of streptavidin molecules. Also, the intensity of Si–O–Si slightly decreases and the intensity of C–H<sub>2</sub> which links the Si–O band to PEG slightly decreases, probably due to the hydrolysis of the Si–O–Si linker when exposed on alkaline water.<sup>36</sup>

Since the OH contents on the surfaces of samples a–d are vastly different (Figure 4), the monolayer attached to the OH group should be significantly different as well. To investigate these differences, the spectra of PEG–biotin and streptavidin-grafted GaN NWs on different samples were compared (Supporting Information s-Figure 3). Curves e and i, respectively, demonstrate biotin functionalization and streptavidin attachment on the piranha-treated GaN NWs. Compared to ALD-TiO<sub>2</sub>, ALD-Al<sub>2</sub>O<sub>3</sub>, and ALD-SiO<sub>2</sub> coating surfaces, the characteristic peaks of PEG–biotin and streptavidin are more attenuated. Furthermore, compared to the characteristic absorbance peaks of PEG–biotin in curve h (sample h: PEG–biotin functionalized ALD-SiO<sub>2</sub> GaN NW), the intensities of those peaks in curves f and g are significantly attenuated. These results are consistent with the OH content shown in Figure 4 and further demonstrate enhanced surface functionalization capability of ALD-coated surfaces, particularly ALD-SiO<sub>2</sub> surfaces. As for streptavidin attached surfaces, there are no significant changes in absorbance peaks shown in curves j–l. It might be due to the detection sensitivity limit of FTIR to show small differences in protein absorbance.

With the attachment of a PEG–biotin monolayer and subsequent attachment of streptavidin molecule, the O–H areas significantly decrease. As shown in Scheme 2, PEG–biotin is grafted on the GaN NW surface by cross-linking with O–H for the attachment of streptavidin molecules. Thus, the consumption of O–H is related to the grafting of the PEG–biotin monolayer

(33) Guo, D. J.; Wang, J.; Tan, W.; Xiao, S. J.; Dai, Z. D. *J. Colloid Interface Sci.* **2009**, *336*, 723.

(34) Meskers, S.; Ruyschaert, J. M.; Goormaghtigh, E. *J. Am. Chem. Soc.* **1999**, *121*, 5115.

(35) Tripp, C. P.; Hair, M. L. *Langmuir* **1995**, *11*, 149.

(36) Guo, D. J.; Xiao, S. J.; Xia, B.; Wang, J.; Pan, Y.; Gu, Z. Z.; You, X. Z. *J. Phys. Chem. B* **2005**, *109*, 20620.

**Table 1. FTIR Frequencies and Assignments of ALD-SiO<sub>2</sub> GaN NWs (Sample d), PEG-biotin Modified SiO<sub>2</sub> GaN NWs (Sample h), and Streptavidin-Grafted PEG-Biotin ALD-SiO<sub>2</sub> GaN NWs (Sample l)<sup>a</sup>**

frequency (cm <sup>-1</sup> )		assignment	
sample d	sample h	sample l	assignment
3361s	3361s	3361s	OH...O stretching from water
3187 m	3190 m	3190 m	OH...O stretching from GaN
2921s, 2850s	2921s, 2850s	2921s, 2850s	asym and sym C—H <sub>3</sub> stretching
	2887 m, 2860w	2887 m, 2860w	asym and sym C—H <sub>2</sub> stretching from PEG
1658s, 1631s	1658s, 1631s	1658s, 1631s	O—H bending
1702vw	1702w	1702w	C=O from the imidazol ring
	1665w	1665w	N—H from the imidazol ring
	1652	1654 m	C=O from biotin or streptavidin
	1543	1546 m	N—H from biotin or streptavidin
1470 m, 1411 m	1470 m, 1415 m	1470 m, 1415 m	C—H bending
1072w	1072 m, 1110s	1072 m, 1110s	Si—O—Si stretching
805w	846s, 805 m	846s, 805 m	Si—O stretching
534s	534s	534s	Ga—N stretching

<sup>a</sup> Abbreviations: sym, symmetric; asym, asymmetric; w, weak; m, medium; s, strong.

**Table 2. Elemental Concentration of N, Ga, Si, Al, and Ti for Samples a, b, c, d, i, j, k, and l**

GaN	N (%)		Ga (%)		Si (%)		Al (%)		Ti (%)	
	weight	atomic								
a	4	18	94	78	2	4	0	0	0	0
b	5	15	75	50	0.4	0.7	20	34	0	0
c	3	12	64	48	1	1	5	9	28	30
d	4	11	64	40	17	26	15	24	0	0
i	10	35	88	62	2	3	0	0	0	0
j	14	37	64	33	0.2	0.3	22	30	0	0
k	14	40	60	35	1	1	3	5	23	20
l	19	42	50	22	22	24	10	11	0	0

and the subsequent attachment of a streptavidin molecule. We have quantified the remaining OH contents using the same method as described above, and listed them in Supporting Information s-Figure 3 and s-Table 1. The OH contents are 0.022, 0.085, 0.091, and 0.041, respectively; and the OH consumptions are 0.074, 0.583, 0.632, and 0.863, respectively. Thus, approximately 77%, 87%, 87%, and 95% of OH contents were consumed. The unreacted OH groups may sit in the inner defect of ALD films, which might be produced during the growth. These OH groups do not have a chance to interact with the reagent. Another OH source may come from hydrolyzation of the unreacted Si—Cl groups. Similarly, for piranha-treated GaN NW, the remaining OH groups probably come from hydrolyzation of the unreacted Si—Cl groups. This result demonstrates that sample l consumes the largest number of O—H functional groups to graft the PEG-biotin monolayer, which subsequently immobilizes streptavidin molecules. Thus, its IR spectrum also presents a denser PEG-biotin component and streptavidin molecule.

### 3.5. HRTEM Imaging of Streptavidin Attachment.

Streptavidin attached on GaN NWs surfaces were dyed with UA and then characterized with HRTEM (Figure 6). Because the major elements of streptavidin molecules, C, N, and O, have relatively low molecule mass, they are not detectable with electronic beams. Therefore, the HRTEM images are thought to be generated by adsorbed U element and the GaN NW. Figure 6i shows a colloid morphology of streptavidin, which stands on the side of GaN NW with thicknesses varying from 10 to 30 nm. According to previous reports,<sup>37</sup> a single streptavidin molecule has a 2D size of  $\sim 5 \times 6$  nm<sup>2</sup>. This colloid layer may be derived from the agglomerate of many streptavidin molecules due to protein denaturalization. After streptavidin is attached to

GaN NWs, we cannot get a clear image of GaN NWs. Figure 6j,k shows protein attachments on Al<sub>2</sub>O<sub>3</sub>- and TiO<sub>2</sub>-coated GaN NWs. Clusters of dark colloids of streptavidin molecules appear on the surfaces of these GaN NWs. However, no clear interface can be identified. Thus, the thicknesses of the streptavidin layers cannot be clearly determined. Unlike for piranha-treated NWs, streptavidin molecules on these ALD surfaces seem to be dispersively coated on the NW surfaces. No complete outline of a streptavidin layer is shown on both pictures. Figure 6l shows protein attachment on the surface of SiO<sub>2</sub>-coated GaN NWs. The image demonstrates that streptavidin molecule aggregates have thicknesses varying from 4 to 30 nm. The smallest one may be a single streptavidin molecule. Different from piranha-treated NWs, most streptavidin molecules on the SiO<sub>2</sub>-coated GaN NWs likely remain globular structures and are not denatured after a series of chemical treatments. It should be noted that a PEG monolayer with molecular weight of 3000 was used here to act as an antifouling film to prevent nonspecific molecule adsorption;<sup>33</sup> therefore, the signals detected here should come from the specific binding of streptavidin and not from the physical adsorption or unspecific binding.

To validate HRTEM results of protein attachments, AFM imaging (Supporting Information s-Figure 4) is used to measure the surface roughness of samples a, i, j, k, and l. Since all GaN NWs including naked GaN NWs and ALD-coated GaN NWs exhibit very smooth surfaces (shown in Figure 1 and 2), the change in the roughness can be attributed to the attachment of streptavidin molecules. AFM results show that all of the protein-grafted surfaces exhibit much higher roughness compared to naked GaN NW surface. This also demonstrates the attachment of streptavidin.

**3.6. Comparing Streptavidin Attachments Using EDX Analyses.** EDX is a semiquantitative method to determine the element concentration. Surfaces a–d were analyzed with EDX to

(37) Cooper, J. M.; Shen, J.; Young, F. M.; Connolly, P.; Barker, J. R. *J. Mater. Sci.* **1994**, *5*, 106.

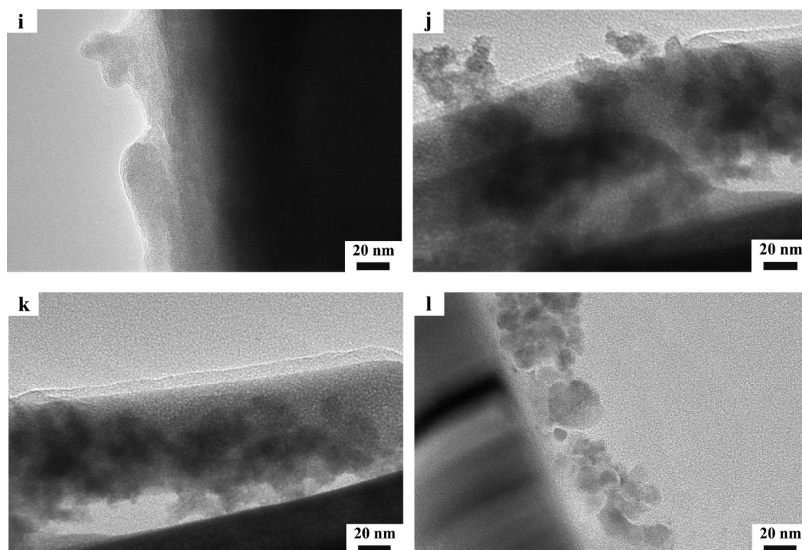


**Figure 6.** HRTEM images of samples i, j, k, and l, streptavidin-grafted NW samples treated with piranha solution, ALD- $\text{Al}_2\text{O}_3$ , ALD- $\text{TiO}_2$  and ALD- $\text{SiO}_2$  coatings, respectively.

compare protein attachments. Figure 7 shows that the emission peaks of N, Ga, Al, Si, and Ti appear at 390, 1120, 1510, 1760, and 4570 eV, respectively. After ALD coating, the concentrations of both N and Ga decrease significantly. Furthermore, compared to ALD- $\text{Al}_2\text{O}_3$  and ALD- $\text{TiO}_2$ , ALD- $\text{SiO}_2$  coated GaN NW shows a more significant decrease in the elemental concentration of Ga, which suggests a higher coating density. These results are consistent with IR results.

EDX analyses also demonstrate the attachment of streptavidin. As changes in C and O elements may be partly attributed to the adsorbed hydrocarbon and air, they cannot be used to evaluate the protein attachment. Because the element N is also one of the main elements in the protein molecule, N is used to determine the streptavidin attachment. Figure 10 demonstrates EDX results of samples i–l. The protein attachments result in a significant increase in the concentration of N and dramatic decreases in the concentrations of Ga, Si, Al, and Ti in all the samples. Quantitative analyses show that N contents in the piranha-treated, ALD- $\text{Al}_2\text{O}_3$ , ALD- $\text{TiO}_2$ , and ALD- $\text{SiO}_2$  GaN NWs increases from 18%, 15%, 12%, and 11% to 35%, 36%, 40%, and 41%, respectively. The changes of N concentration on surfaces i–l (7%, 21%, 28%, and 31%, respectively) are likely due to the attachment of streptavidin. Additionally, Ga concentrations in the piranha-treated, ALD- $\text{Al}_2\text{O}_3$ , ALD- $\text{TiO}_2$ , and ALD- $\text{SiO}_2$  GaN NWs decrease from 78%, 50%, 48%, and 40% to 62%, 33%, 35%, and 22%, respectively. Decrease in the Ga concentration may be derived from the ALD coating and the addition of a large quantity of N. All these results demonstrate that streptavidin has been successfully attached to all the functionalized GaN NW surfaces. On the basis of the changes in the atomic concentrations of N and Ga elements, we can determine the amount of attached streptavidin film, changing in film thickness or density. Using this approach, we compared the thicknesses of streptavidin film among the four types of samples and ranked the functionalization capability of these surfaces from the highest to the lowest: ALD- $\text{SiO}_2$ , ALD- $\text{TiO}_2$ , ALD- $\text{Al}_2\text{O}_3$ , and piranha-treated GaN. These results are consistent with the FTIR and fluorescent results.

### 3.7. Fluorescent Imaging of Streptavidin Attachment.

For fluorescent imaging, Cy3-labeled streptavidin was used to bind to the surfaces of PEG–biotin-grafted GaN NWs. The

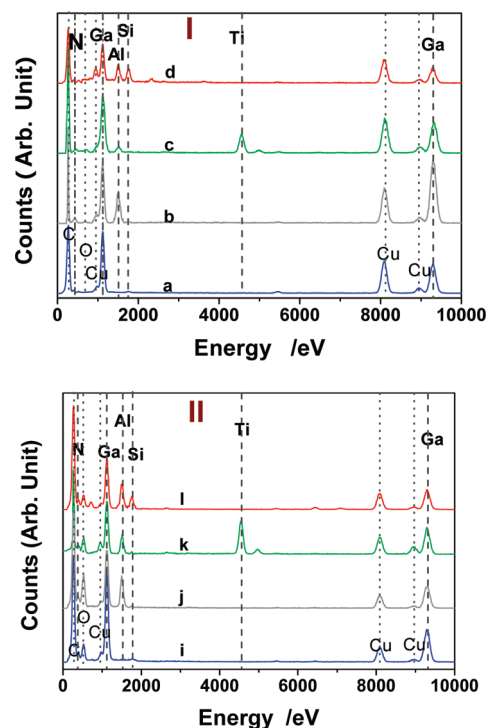


**Figure 7.** Energy-dispersive X-ray microanalysis of samples a–d (I) and samples i–l (II).

fluorescent intensity of streptavidin molecules was thus used to quantify the density of the attached proteins, which was correlated with the density of functional groups. Figure 8i–l shows protein attachments to laid-down GaN NWs. Clearly, all four pictures exhibit the characteristic fluorescence of Cy3. These figures demonstrate that Cy3-labeled streptavidin molecules were immobilized onto all the four samples. Among these samples, significant differences exist in the fluorescent intensity or the grafting density. The mean fluorescent intensities for samples 8i–l are 17, 109, 133, and 167, respectively. This change is also plotted in Figure 9. The fluorescent intensities of samples j, k, and l are significantly higher than that of sample i, approximately 6.4, 7.8, and 9.8 times, respectively. Additionally, the fluorescent intensity

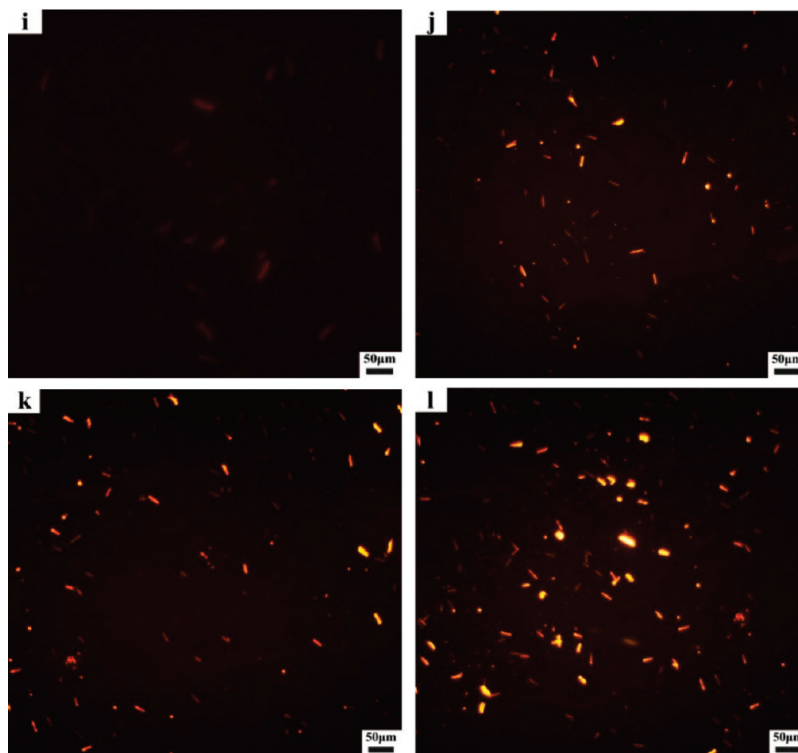


**Figure 8.** Fluorescence images of samples i, j, k, and l. The four samples are treated and imaged at exactly the same conditions.

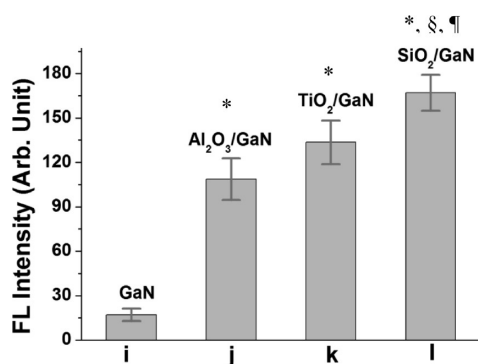


**Figure 9.** Comparison of fluorescent intensity on samples i, j, k, and l. \*: significantly different ( $p < 0.05$ ) from GaN (sample i). §: significantly different ( $p < 0.05$ ) from sample j. ¶: significantly different ( $p < 0.05$ ) from sample k. The error bars indicate the standard error of the mean.

of sample l is significantly higher than that of sample j and that of sample k. This result is consistent with the FTIR, HRTEM/EDX, and AFM results shown above. Supporting Information s-Figure 5 shows protein attachments to the arrays of upright GaN NWs on the chip, with each dot representing a single upright GaN NW. As comparison, Figure i-2 in s-Figure 5 exhibits the fluorescent image showing protein attachments to bare GaN grown upright on the chip. A dark red fluorescent signal was found, which may be derived from both unspecific and specific adsorption of streptavidin. Figure l-2 in s-Figure 5 exhibits a bright red fluorescent image showing protein attachments to sample l which remains on the chip array. These results using as-grown NW chips further confirm the successful attachment of streptavidin molecules on NWs on a chip array format.

**3.8. Relationship of the N Concentration and Fluorescent Density with OH Consumption.** Herein, the O–H consumption is used to estimate the cross-linking degree, and the changes

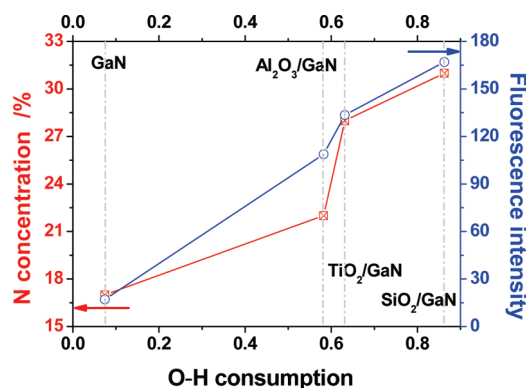


**Figure 10.** Relationship of the N concentration change and the fluorescent density to the O–H consumption on samples i–l. The consumption of O–H equals the original O–H content from ungrafted GaN NW subtracting the remaining O–H content from the streptavidin-attached sample. The net change in N concentration equals the N concentration from the streptavidin-attached sample subtracting the N concentration from ungrafted GaN NW.

of N concentration from EDX analyses and the fluorescence intensity of streptavidin are used to estimate streptavidin attachment. Figure 10 plotted the N concentration change and the fluorescence intensity against the O–H consumption on samples i, j, k, and l. As expected, with the increase in cross-linking degree from sample i to sample j, to sample k, and to sample l (highest degree), both the N concentration change and the fluorescence intensity exhibit an increasing trend. This suggests that IR detection, fluorescence scanning, and EDX/TEM observation are highly consistent.

#### 4. Conclusion

We have successfully coated three kinds of ALD coating films, i.e., TiO<sub>2</sub>, Al<sub>2</sub>O<sub>3</sub>, and SiO<sub>2</sub>, on the array of upright GaN NWs. Results showed that more OH groups were present on the three

ALD-coated NWs compared to the piranha-treated GaN NW. Results also showed that, after subsequent silanization and probe grafting on these NW substrates, denser target proteins were found to attach onto the ALD-coated NWs compared to the piranha-treated GaN NW. Among the three ALD coatings, SiO<sub>2</sub>-ALD showed a thicker or denser film and yielded more promising results in OH content and protein attachment. We have thus demonstrated for the first time that ALD coating can be used as a high-potential functionalization strategy for nanobiosensors, because it is capable of creating functional groups with much higher density compared to that of acid-based modifications.

**Acknowledgment.** The authors would like to thank Dr. Shao-Jie Fu for helping with FESEM imaging and Mrs. Zhi-Ping Zhou for HRTEM imaging. This work was supported by YFA HR0011-08-1-0041 (W.T.), DARPA Center on Nanoscale Science and Technology for Integrated Micro/Nano-Electromechanical Transducers (iMINT) funded by DARPAN/MEMS S&T Fundamentals Program (N66001-10-1-4007) (Dr. D. L. Polla, Program Manager), and National Natural Science Foundation in China no. 50805076.

**Supporting Information Available:** Additional graphics and data as described in the text. This material is available free of charge via the Internet at <http://pubs.acs.org>.